

Supplementary information

Piezotronic effect boosted photocatalytic performance of Bi₂NdO₄Cl for degradation of organic pollutants

Kai Lin, Xiaoyi Dong, Liang Xu, Qi Wang, Jiajing Wang, Yongjin Li*, Zhaoyi

Yin, Jin Han, Jianbei Qiu, Zhiguo Song*

*School of Materials Science and Engineering, Kunming University of Science and
Technology, Kunming, 650093, China*

*Corresponding Author

E-mail addresses: liyongjin@kust.edu.cn (Y. Li); songzg@kust.edu.cn (Z. Song)

Table of content

1. Preparation of catalyst
2. Characterizations
3. Catalytic performance test
4. *Fig. S1* - XPS survey spectrum of BNOC sample
5. *Fig. S2* - Piezo-photocatalytic performance of TH degradation by harvesting multisource energies from light (NIR) and stirring vibration
6. *Fig. S3* - Transient photocurrent response of BNOC with on-off cycles of light, light + stirring in 0.5 mol L⁻¹ Na₂SO₄ solution (Experimental conditions: stirring speed=600 rpm)
7. *Fig. S4* - (a) Piezo-photocatalytic degradation curves and (b) the corresponding *k* values of BNOC sample for TH solutions with different catalyst dosage
8. *Fig. S5* - UV-vis absorption spectra of (a) MB, (b) CIP and (c) TH aqueous solutions

at different time of degradation over BNOC piezo-photocatalyst. (d) Variation of dye (antibiotic) concentration as a function of time

9. *Fig. S6* - (a) Band structure and (b) partial and total density of states (PDOS and TDOS) for BNOC

Experimental

1. Preparation of catalyst

The $\text{Bi}_2\text{NdO}_4\text{Cl}$ was synthesized by the conventional solid stated reaction process. Firstly, BiOCl was prepared by the following method: Bi_2O_3 and NH_4Cl were mixed with appropriate stoichiometric amounts in a logical order and grinded thoroughly for over 30 min in an agate mortar. After that, the grinded mixtures were placed in an alumina crucible and calcined at 500°C for 4h, while the heating rate was $5^\circ\text{C}/\text{min}$. Secondly, bismuth oxide (Bi_2O_3 , 99.99%), bismuth oxychloride (BiOCl) and neodymium oxide (Nd_2O_3 , 99.99%) at the stoichiometric molar ratio of 1:2:1 were ground for 60 min. The mixture was placed in an alumina crucible with a capacity of 30 cm^3 and heated at 1073 K for 12 h^{1,2}.

2. Characterizations

The phase structures were observed by the X-ray diffraction measurements using an Ultima IV diffractometer with $\text{Cu K}\alpha$ radiation ($\lambda=1.5406\text{\AA}$, $U=40\text{kv}$, $I=40\text{mA}$). The

morphology and microstructure were examined by field emission scanning electron microscope (Hitachi Regulus8100, Japan) and transmission electron microscopy (TEM, FEI Tecnai G20). Meanwhile, the chemical compositions and mapping images of the products were employed by the energy dispersive spectrum (EDS), which was attached to the SEM. To analyze the chemical states and surface composition of samples, the X-ray photoelectron spectroscopy (XPS) measurement was done on a Thermo Scientific K-Alpha spectrometer using 150W Al K α X-ray sources, and all the binding energies were referenced to the C1s peak at 284.8 eV of the surface adventitious carbon. UV–vis diffuse reflectance spectra (DRS) were recorded on a Hitachi U-4100 spectrophotometer equipped with a 150W xenon lamp as the excitation source, using BaSO₄ as a reference. Electrochemical properties were characterized by an electrochemical workstation (Reference 600+) with a Pt counter electrode, an Hg/Hg₂Cl₂ as reference electrode, and 0.5 mol L⁻¹ Na₂SO₄ solution as the electrolyte. The piezoresponse force microscopy (PFM, Bruker Multimode 8, USA) was used to observe the topography and piezoelectric response of the sample.

3. Catalytic performance test

3.1 Photo-/piezocatalytic performance test

The photo-/piezocatalytic performance of the BNOC samples was assessed by a home-made photochemical reaction system and the system temperature was maintained at 25° C by cooling water circulation. In this measurement, a 500 W Xe lamp was employed as solar simulator to provide sunlight source (full-spectrum light), and flowing was simulated through a speed-adjustable stirring module with an adjustable

speed in the range of 200-1400 rpm to provide mechanical stress on the samples. Typically, 20 mg BNOC was dispersed in 40 ml TH aqueous solution ($C_0 = 10$ mg/L), after that the suspension was equilibrated in the dark for a period of time to reach adsorption-desorption equilibrium. After stirring treatment and/or sunlight irradiation, 3.5 ml suspension was removed every 20 minutes and then centrifuged to obtain the supernatant. The concentration of tetracycline hydrochloride was identified by measuring the photoabsorption intensity at the wavelength of 356 nm.

3.2 Recyclability and stability test

20 mg of the as-prepared photocatalytic material was weighed and placed in a glass container, then 40 mL of tetracycline hydrochloride solution ($C_0=10$ mg/L) was added. After that, the suspension was equilibrated in the dark for a period of time to reach adsorption-desorption equilibrium. After co-utilizing stirring(1400rpm) and sunlight irradiation, 3.5 ml suspension was removed every 20 minutes and then centrifuged to obtain the supernatant. The concentration of tetracycline hydrochloride was determined by measuring the photoabsorption intensity at the wavelength of 356 nm. After each recycles, the supernatant was poured out from the reaction vessel and the remaining photocatalytic material was dried. Subsequently, 40 mL of tetracycline hydrochloride was added again and the process was repeated six times.

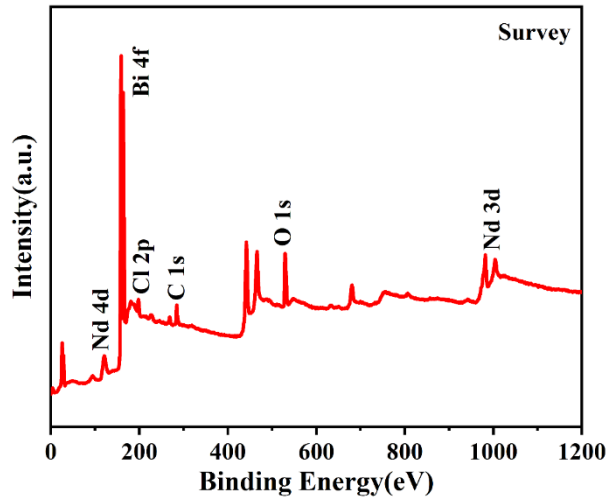


Fig. S1 XPS survey spectrum of BNOc sample.

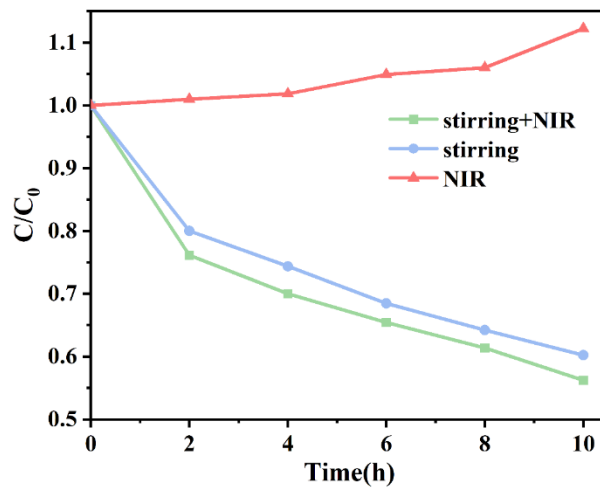


Fig. S2 Piezo-photocatalytic performance of TH degradation by harvesting multisource energies from light (NIR) and stirring vibration.

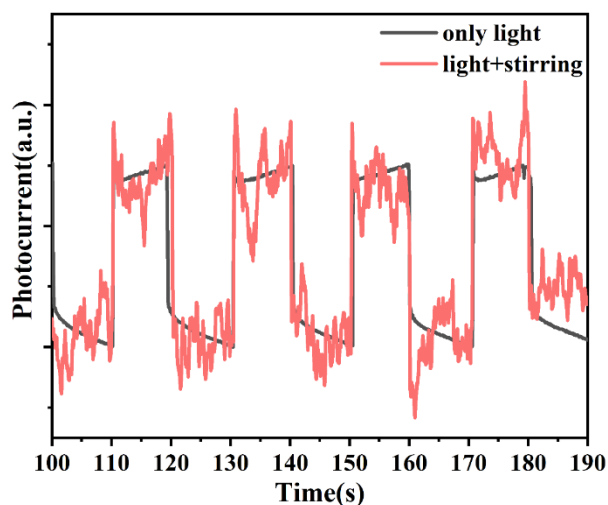


Fig. S3 Transient photocurrent response of BNOC with on-off cycles of light, light + stirring in $0.5 \text{ mol L}^{-1} \text{ Na}_2\text{SO}_4$ solution (Experimental conditions: stirring speed=600 rpm).

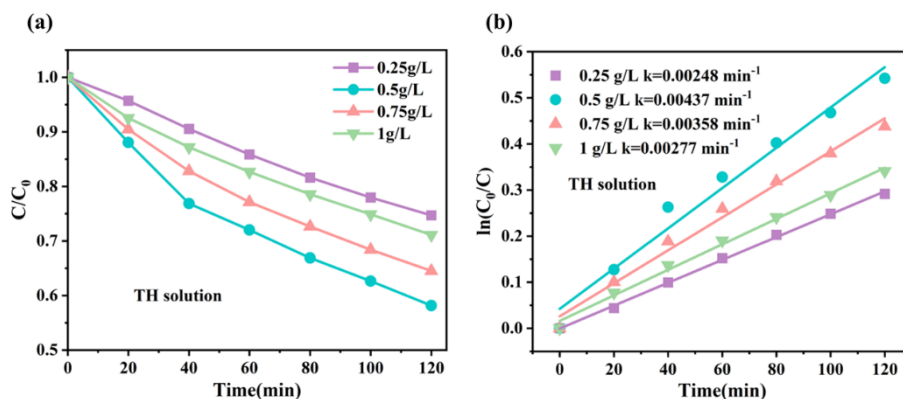


Fig. S4 (a) Piezo-photocatalytic degradation curves and (b) the corresponding k values of BNOC sample for TH solutions with different catalyst dosage.

The dependence of degradation efficiency on the amount of the catalyst is shown in Figure S4 a. The optimal concentration of BNOC is around 0.5g/L. Further increase in the amount of catalysts has led to the reduction of piezo-photocatalytic efficiency. Accordingly, the calculated k values increase first and then decrease with the increasing

amount of the catalyst, as shown in Figure S4 b. Similar to the previous report³, the phenomenon can be attributed to higher probability of collisions between sheets and sheets with the increase of the amount of catalyst, which may lead to the neutralization of surface charges. Furthermore, a higher solid loading possibly leads to a reduced absorption density of the TH at the surfaces in a BNOC dispersion. This in turn results in a reduced surface-charge density at the BNOC sheet in an aqueous dispersion and possibly enhances the degree of agglomeration.

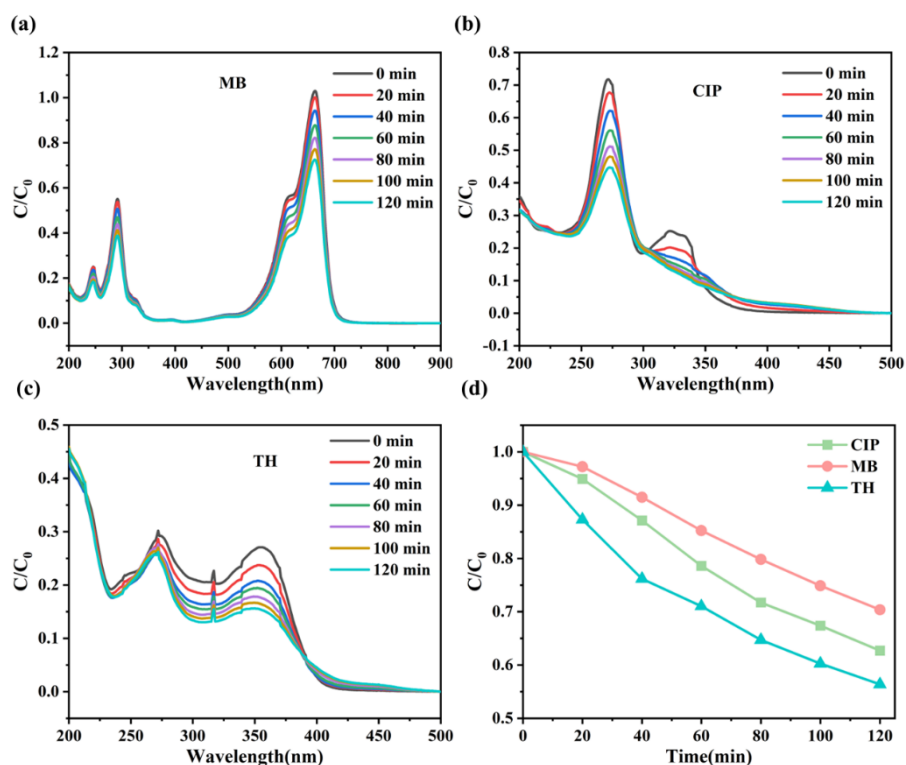


Fig. S5 UV-vis absorption spectra of (a) MB, (b) CIP and (c) TH aqueous solutions at different time of degradation over BNOC piezo-photocatalyst. (d) Variation of dye (antibiotic) concentration as a function of time.

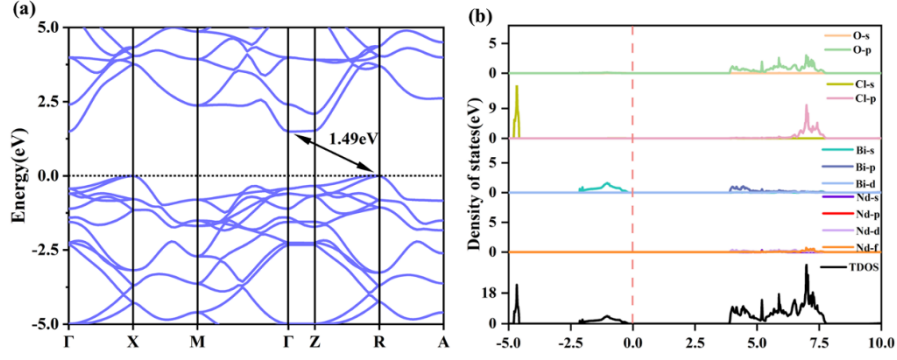


Fig. S6 (a) Band structure and (b) partial and total density of states (PDOS and TDOS) for BNOC

The calculations of band structure were performed based on the density functional theory (DFT) simulations with the Vienna ab initio simulation package (VASP). The core-valence interactions were treated by the projector augmented wave (PAW) method, where the plane wave expansion was truncated with a cutoff energy of 520 eV. To better determine the value of band gap, a k-points grid with $(7 \times 7 \times 3)$ was used in self-consistent calculations for the structure optimization. Based on the calculation results, the valence band maximum and the conduction band minimum lie on the R and Γ points, respectively. Hence, this shows the indirect band gap nature. The calculated band gap value (1.49 eV) of BNOC is narrower than experimental results by UV-Vis-NIR absorption spectra (1.7 eV), which may be resulted from the well-known limitation of generalized gradient approximation (GGA). Moreover, the density of state (DOS) plots manifest that the Bi 6s and Cl 3s participate in electronic hybridization in the VBM of $\text{Bi}_2\text{NdO}_4\text{Cl}$, while the CBM of $\text{Bi}_2\text{NdO}_4\text{Cl}$ mainly consists of O 2p, Bi 6p, Cl 3p and the electrons of Nd atoms.

Reference

- 1 N. Han, S. Xu and Q. Zhang, *J. Mater. Sci.*, 2022, **57**, 2870-2882.
- 2 X. Wang, J. Ran, M. Tao, Y. He, Y. Zhang, X. Li and H. Huang, *Mater. Sci. Semicond. Process.*, 2016, **41**, 317-322.
- 3 J. Wu, W. Mao, Z. Wu, X. Xu, H. You, A. Xue and Y. Jia, *Nanoscale*, 2016, **8**, 7343-7350.